Tannic acid self-aggregation and adsorption onto a polyethersulfone membrane: An all-atom molecular dynamics study

Marie Certiat, Johanne Teychené, Christelle Guigui, Stephanie Laborie, Franck Jolibois

Journal of Membrane Science 697 (2024) 122570

Contents lists available at ScienceDirect

Journal of Membrane Science

journal homepage: www.elsevier.com/locate/memsci

Tannic acid self-aggregation and adsorption onto a polyethersulfone membrane: An all-atom molecular dynamics study

Marie Certiat [a,b], Johanne Teychené [b], Christelle Guigui [b], Stéphanie Laborie [b], Franck Jolibois [a,*]

[a] LPCNO, UPS, CNRS (UMR 5215), Institut National des Sciences Appliquées (INSA), Université de Toulouse, 135 Avenue de Rangueil, F-31077, Toulouse, France
[b] Toulouse Biotechnology Institute (TBI), Université de Toulouse, CNRS, INRAE, INSA, Toulouse, 31077, France

ARTICLE INFO

Keywords:
Ultrafiltration
Fouling
Molecular dynamics
Tannic acid
Polyethersulfone

ABSTRACT

Atomic scale modeling is crucial for characterizing the interactions responsible for fouling, which is a major limitation in the use of membrane filtration technologies for the recovery of polyphenols. In this work, a methodology to model a porous ultrafiltration polyethersulfone (PES) membrane is presented. Subsequently, various systems containing tannic acid (TA) molecules at different concentrations (9 or 30 g/L) were studied, with two additional systems incorporating a PES membrane, through 100 ns all-atom molecular dynamics simulations. The results show that up to 90% of the TAs are self-aggregated, associated with the formation of intermolecular H-bond and π-stacking interactions. Furthermore, adsorption of 48–67% of the TAs onto PES was observed. TA-PES H-bond and π-stacking interactions are also formed. The number of adsorbed TAs molecules over time and the evolution of the mean size of TA aggregates exhibits similar temporal trends, suggesting a parallel progression in both phenomena. Moreover, the same atoms were involved in both aggregation and adsorption, leading to the conclusion that the two phenomena compete. These results shed light on the fouling mechanism, which appears to occur through the formation of a cake layer combined with adsorptive fouling, and could support the design of new antifouling agents adapted for polyphenol filtration.

1. Introduction

The rising interest in recovering bioactive compounds from biomass, particularly polyphenols, is attributed to their wide range of applications in pharmaceuticals, food, and cosmetics [1,2]. Among these compounds, tannic acid (TA), the best known hydrolysable tannin [3], found in various plant materials [4], stands out due to its numerous health benefits, including antioxidant, anti-inflammatory, anti-bacterial, anti-viral, and anti-tumor properties [5]. Extracting TA and other polyphenols from biomass is therefore of great interest for the development of new pharmaceutical products and dietary supplements.

Conventional polyphenol extraction from plants via solid-liquid methods faces limitations due to the use of large amounts of costly and environmentally unfriendly organic solvents [6,7]. In this context, ultrafiltration (UF) membranes present an appealing alternative for separating polyphenols, offering advantages in reduced energy and solvent consumption [8–11]. However, the use of UF membrane is limited by membrane fouling, a complex phenomenon encompassing various mechanisms including foulant adsorption, cake/gel formation, complete or intermediate/partial pore blocking and internal/standard pore blocking [12–15]. Multiple factors, including membrane materials and molecular weight cut-off (MWCO), solute nature and concentration, significantly influence membrane fouling through specific solute-membrane interactions.

Polyethersulfone (PES) membranes, adhering to food-grade standards [16], are renowned for their good chemical, thermal and mechanical resistances [17,18]. Several studies have focused on the recovery, separation, fractionation and/or concentration of polyphenols by a PES UF membrane [19–25]. Recently, Manios et al. [26] studied the decaffeination of ground coffee brews by a tight PES UF membrane with a MWCO of 2 kDa. They successfully separate caffeine from polyphenols, with 87% of polyphenols rejection ratio. Despite the presence of large macromolecules in the feed solution, the flux reduction was only 60% and remained stable throughout the process. Insights into the intricate fouling mechanism of PES membranes can be obtained by varying MWCO. Cifuentes-Cabezas et al. [27] studied two hydrophilic PES membranes with 4 and 50 kDa MWCO. They observed that membranes with a higher MWCO were more affected by the adsorption of polyphenols, followed by gel layer formation, leading to severe fouling. Sánchez-Arévalo et al. [28] reached similar conclusions when

* Corresponding author. LPCNO, Université Fédérale De Toulouse Midi-Pyrénées, INSA-CNRS-UPS, 135 Avenue De Rangueil, 31077, Cedex 4, Toulouse, France.
E-mail address: franck.jolibois@univ-tlse3.fr (F. Jolibois).

https://doi.org/10.1016/j.memsci.2024.122570
Received 13 December 2023; Received in revised form 8 February 2024; Accepted 12 February 2024
Available online 13 February 2024

comparing two PES membranes with MWCO of 5 and 30 kDa, supporting the fact that membranes with low MWCO appear to be protected against pore blocking. These results underline the complex mechanism of PES membrane fouling by polyphenols, involving adsorptive fouling, pore blocking, and gel layer formation. In addition, other studies have investigated PES fouling by modifying membrane hydrophilicity. Chu et al. [29] demonstrated that enhancing membrane hydrophilicity, achieved via graphene-oxide coatings, correlated with reduced permeate flux reduction. The presumed TA adsorption onto the PES membrane could lead to reduced membrane pore size and thus promote the formation of a cake layer responsible for reversible fouling. They suspected that the formed TA layer is made of weak interactions, explaining why back-washing can restore the membrane flux by breaking this layer. On the contrary, Cai et al. [30] highlighted the antifouling ability of hydrophobic PES membranes. Nonetheless, they observed important polyphenol adsorption, attributing it to π-stacking and hydrogen bonding interactions. These observations highlight the crucial role of solute-membrane interactions in fouling phenomena and the importance of in-depth exploration. El Rayess et al. [31] proposed a unique fouling mechanism involving rapid tannin adsorption onto PES membranes, followed by pore-level aggregation, potentially resulting in pore blocking and cake layer formation. In fact, the self-aggregation of tannins [32–34], especially TA [35,36], have been clearly identified by Dynamics Light Scattering and Nanoparticle Tracking Analysis. TA self-aggregation results in the formation of colloidal particles several hundred nanometers in size, depending on solution chemistry, such as solute concentration. This aggregation might significantly contribute to PES membrane fouling by generating particles exceeding pore sizes or facilitating cake layer formation, necessitating comprehensive investigation. In summary, UF PES membranes hold promise in recovering polyphenols, especially TA. However, fouling is a complex mechanism, dependent on specific system composition and conditions. To improve operating conditions, design better membranes, and develop effective fouling control strategies, characterization at the atomistic-level of membrane-solute and solute-solute interactions is essential to address fouling limitations.

In this context, molecular dynamics (MD) simulations appear as a method of choice to study, at the molecular level, the factors that govern the solute-membrane interactions involved in the fouling process and support the experimental results, as reported in recent reviews [37,38], especially between membranes and polyphenols [39]. Notably, some studies have modeled PES membranes and established the foulant-membrane interactions. Ahn et al. [40] have studied fouling through a system composed of a bulk PES structure, composed of a polymer chain of 60 repeating units, and a model of humic acid with two phenolic groups. They conjectured that the simulation times of 0.3 ns were insufficient, precluding the observation of any specific membrane-foulant interaction. Arandia et al. [41] also modeled a PES membrane, made of a PES chain of 200 monomers, to evaluate the fouling behavior of cellulose, through 6 ns MD simulations. They determined the attractive and repulsive forces are involved in foulant-foulant and membrane-foulant interactions and demonstrated that the adsorption is exothermic, proposing temperature control to reduce fouling. Finally, Virtanen et al. [42] have studied the adsorption of up to 50 molecules of vanillin, a small phenolic compound, onto a PES membrane, made of 100 PES dimers, through 320 ns MD simulations. These simulations revealed that hydrophobic and H-bond interactions are at the origin of vanillin adsorption. In summary, the existing theoretical studies on characterizing PES membrane-foulants interactions have certain limitations. Some studies only investigate small phenolic compounds, while others are conducted on small systems for short periods of time. Additionally, all these simulations restrict the membrane modeling to bulk PES structures.

To address these research gaps, this study presents the outcomes of all-atom MD simulations aimed at assessing fouling-related interactions in larger systems, containing a polyethersulfone ultrafiltration membrane and tannic acid, selected as a representative polyphenol of intermediate size. Initially, TA self-aggregation was investigated on two large-scale systems, each containing 15 or 50 TA molecules, corresponding to concentrations of 9 or 30 g/L, respectively, to evaluate the influence of TA concentration. Subsequently, a PES membrane was introduced into the aforementioned systems to evaluate the TA-PES interactions responsible for TA adsorption. Consequently to the large size of the TA-containing systems, a large PES membrane was constructed, made of 87 chains, each comprising 40 repeating units, significantly surpassing those previously explored. Importantly, this PES model incorporates UF-sized pores, implemented at the all-atom MD level for the first time, paving the way for future innovative simulations such as the transport of polyphenols through PES. However, this PES model aims not to identically replicate a complex experimental membrane but rather to adequately portray TA-PES interactions. These simulations offer novel insights into the fouling mechanism of PES membranes by polyphenols, making significant contributions to the field and guiding the development of new strategies to mitigate fouling issues.

2. Materials and methods

2.1. Experimental

To validate the force field parameters used and the resulting PES and TA models, theoretical and experimental IR spectrum were compared, as well as the density of the membrane.

2.1.1. Reagents

Tannic acid ($C_{76}H_{52}O_{46}$, 1701.2 g/mol) was purchased from Sigma Aldrich (Merck, USA) and Polyethersulfone ultrafiltration membrane (Molecular Weight Cut Off of 100 kDa) was provided by MiliporeSigma (Merck, USA). Milli-Q water (18.2 MΩ .cm) was used.

2.1.2. ATR-FTIR

The spectrum of tannic acid in ultra-pure water and of the PES membrane were obtained using an ATR-FTIR (PerkinElmer, UK). Before measurement, PES membranes were immersed in ultrapure water for 24 h to remove preservatives, then dried in a speed vacuum at 30 °C for 4 h. Scanning was done in a range of 4000 - 450 cm^{-1} at a resolution of 4 cm^{-1}. The spectrum obtained was an average of 100 scans.

2.1.3. Density

Membrane density was calculated by averaging the dimensions and mass of 5 membranes, measured on a Sartorius balance with an accuracy of ±0.1 mg. Prior to measurement, the membranes were dried in an oven at 30 °C for 24 h.

2.2. Computational methods

2.2.1. Parameters of simulations

All-atom classical molecular dynamics (MD) simulations were performed using the NAMD software [43]. The interactions potential and energy gradients were described with the General AMBER Force Field (GAFF) [44]. The antechamber program [45], part of the AmberTools package, was used to calculate the partial charges of PES and TA atoms using the RESP charges method calculated at the HF/6-31G* level using the Gaussian09 software [46]. TIP3P [47] model was employed to describe water molecules.

The simulations were performed in rectangular boxes with periodic boundary conditions (PBCs) imposed in all the directions. A 20 Å cut off was applied to calculate the van der Waals and electrostatic non-bonded interactions. Particle Mesh Ewald summation was applied to calculate full electrostatic interactions between atoms. All simulations followed the same initialization procedure before the production runs. First, energy minimization was performed for 5000–10,000 steps according to

the size of the system using the conjugate gradient algorithm. The systems were then heated from 5 to 295 K in steps of 5 K for a total simulation time of 295 ps with an integrator time step of 1 fs in the NVT ensemble. After this initialization procedure, MD simulations were run in the NVT and/or NPT ensemble at 295 K with a time step of 1 fs. To overcome convergence problems that appeared at the beginning of simulations, it was necessary to punctually use smaller or larger time steps ranging from 0.5 to 2 fs. Velocity Verlet propagator was used to solve the equations of motions. Langevin thermostat was used to control the temperature during NVT simulations. NPT simulations were executed by adding a Nosé-Hoover Langevin piston pressure control, with a constant pressure of 1 atm.

2.2.2. TA and PES building

Tannic acid (TA) is a complex molecule composed of a glucose core, covalently bound through ester linkage to ten units of gallic acid. The nomenclature used for TA atoms in the present study is described in Figure S1a. Its initial structure was built using the Jmol software [48] and subjected to full geometry optimization at the HF/6-31G* level owing to the Gaussian09 suite of programs. The optimized structure was subsequently used as the initial configuration for all molecular systems used in the MD simulations.

The swelling of filtration membranes is known to have an important impact on the membrane structure. Recent studies have focused on modeling membrane swelling, by using special protocols such as simulated annealing [49,50] or non-equilibrium MD with walls acting as pistons [51,52] to facilitate water penetration. However, studies on various hydrophobic membranes, including PIM, PBI, and PI, have consistently reported marginal polymer dilation and limited pore expansion upon swelling in water, with swelling factor being nearly unit and mostly attributed to water sorption [49,52]. As a consequence, because the PES membrane is also hydrophobic, a more straightforward method was applied in this study to model membrane hydration, not applying specific swelling protocols to decrease the computational cost.

A polyethersulfone (PES) polymer chain (Figure S1b) was created from 40 repeating monomer units using the LEAP program of the AMBER suite [53]. This PES chain has a molecular weight of 9.46 kDa, in the same order of magnitude of commercial PES membrane of 20–150 kDa [54]; a more extensive discussion about the length of the PES chain used in this study can be found in the description of Figure S2. The chain was capped with a C_6H_5 phenyl group on one side, and an O–C_6H_5 group on the other (Figure S2). Then, 87 polymer chains were placed randomly in a simulation box using the Packmol program [55]. Because the PES chains were initially unfolded, a larger initial box size was set up (397 Å × 394 Å × 400 Å). After the initialization procedure described above, a first NVT run of 3.9 ns was performed, followed by a 19.6 ns simulation in the NPT ensemble, leading to a stabilized box size of 179 Å × 178 Å × 180 Å, corresponding to an intermediate PES model with a density of 0.26. PBCs have been imposed in all the MD simulations. Figure S3 and Video S1 illustrate the construction steps.

Subsequently, water was added to system. A layer of water containing 151,000 molecules was placed above the membrane along the z-axis using Packmol. After 6.7 ns of NPT production, a 159 Å × 160 Å × 213 Å simulation box was obtained, containing a top layer of water with a thickness of ~60 Å, and the remaining water was uniformly distributed around the membrane (Fig. 1).

2.2.3. Validation of models and associated forcefield parameters

To validate the constructed PES and TA models and the associated force field parameters used in the simulations, theoretical calculation of the InfraRed (IR) spectrum of these molecules was undertaken and compared to experimental FTIR-spectra.

The previous equilibrated system containing the membrane in water (Fig. 1) was used to compute the IR spectrum of PES. The simulated spectrum of TA was obtained from a system containing one TA molecule and 3462 water molecules. This last system was equilibrated for 10 ns in the NVT ensemble and then for 2.5 ns in NPT, with a final box size of 49 Å × 46 Å × 45 Å. The theoretical IR spectra of PES and TA were calculated for wavenumbers ranging from 500 to 5000 cm^{-1}, corresponding to a period of vibration modes ranging from 7 to 70 fs. After the initialization procedure, simulations in the NVT ensemble were run for 25 ps, for each system, which is more than 300 times higher than the slowest normal modes, allowing good sampling of vibration frequencies. The timestep was set to 0.5 fs, and frames were extracted every 2.5 fs, which is more than 2 times smaller than the fastest observed frequencies.

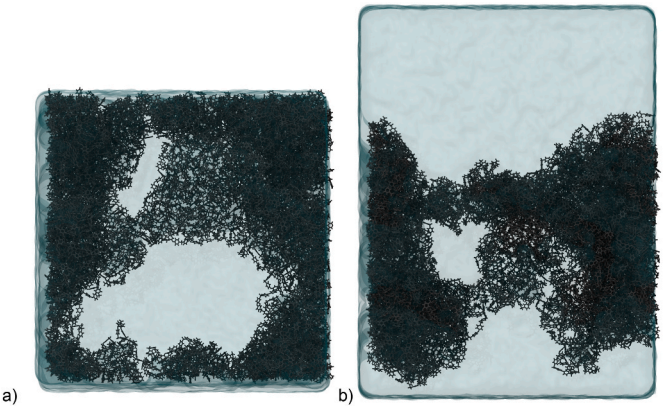

Fig. 1. Final structure of the PES membrane in pure water. The PES is displayed in gray and water is displayed in QuickSurf representation in cyan. a) Top view of the PES membrane. Two pores are visible, perpendicular to the membrane surface, of 8 and 13 nm maximum length and b) Side view of the PES membrane. More snapshots of the PES membrane are presented in Figure S4. (For interpretation of the references to color in this figure legend, the reader is referred to the Web version of this article.)

Theoretical IR spectra were obtained using the Fourier transform of the dipole moment autocorrelation function computed from MD simulations data [56]. Each peak was subsequently convoluted with a Gaussian function using an arbitrary full width at half maximum, leading to a final spectrum comparable to that of the experiment. As it is usual for the calculation of vibrational spectra by quantum chemical methods [57–59], a scaling factor has been applied (0.94 and 0.88, for TA and PES, respectively), to match the best experimental spectra. The theoretical IR spectra obtained for PES and TA are shown in Fig. 2. Table S1 summarizes the comparison of the experimental and theoretical peaks of the IR spectra. As reported in Table S1, the average absolute deviation between theoretical and experimental IR spectra is 18 and 13 cm^{-1} for TA and PES, respectively. For both compounds, the largest variation compared to experiment was only 42 cm^{-1}. The variations that have been identified are consistent in magnitude with those that have been documented in previous research, particularly in studies that have employed more precise methods [60,61]. Given this background, it can be asserted with assurance that the spectra of both PES and TA are in very good agreement with the experimental ones.

The TA and PES models used allow a qualitative (almost quantitative) reproduction of the experimental IR spectra, thus validating the parametrization of the forcefield used for these models for further theoretical studies.

To validate the structure of the theoretical PES membrane, several parameters have been evaluated. The structure of the PES was impacted by the presence of water and compacted during the last NPT run (as described section 2.2.2), resulting in a final PES membrane with pore sizes ranging from ~3 to ~13 nm (Fig. 1), consistent with the pore size of the UF membranes ranging from 1 to 50 nm [62]. The volume occupied by the PES membrane was calculated without taking into account the top layer of water, resulting in a PES density of 0.34. This theoretical density is in qualitative agreement with the density of the PES UF membrane of 0.47, measured experimentally (see Materials and

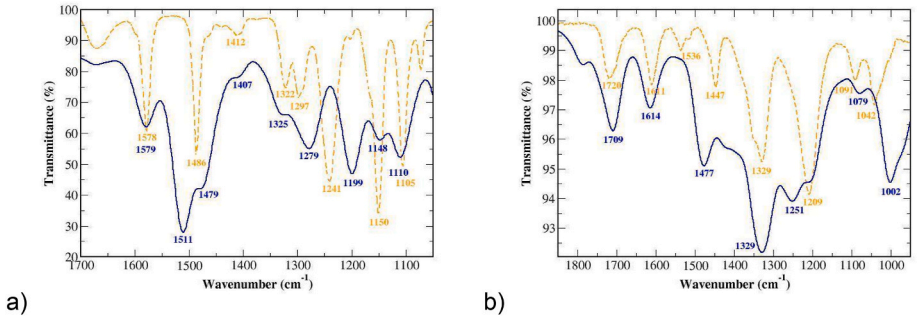

Fig. 2. Comparison of theoretical (solid blue line) and experimental (dashed orange line) Infrared Spectra obtained from a) PES in water and b) TA in water. (For interpretation of the references to color in this figure legend, the reader is referred to the Web version of this article.)

methods 2.1.3). Moreover, the surface porosity of the PES model was computed based on snapshot shown in Fig. 1a using ImageJ [63], resulting in a theoretical PES surface porosity of 21.0%, in good agreement with the experimental porosity of a commercial PES with a MWCO of 100 kDa ranging between 10.5 and 27%, according to different sources [64,65]. To our knowledge, this is the first time that a porous ultrafiltration membrane was modeled at the atomic scale level.

2.2.4. Complete systems construction

In an attempt to understand the influence of several parameters on the TA-TA aggregation and TA-PES adsorption phenomena, several systems have been set up. First, the effect of TA concentration was studied by creating two systems composed of 15 or 50 TA molecules solvated in pure water, leading to a concentration of 9 or 30 g/L, respectively. In a second step, the influence of the PES membrane was analyzed by adding a PES membrane to the two previous systems. In all these systems, each TA molecule was placed in a random position in the simulation box using the Packmol program. Table S2 summarizes the compositions of these different systems. For all the systems, the TA concentration was calculated according to the number of water molecules in the system and not by considering the volume of the simulation box, to prevent taking into account the volume occupied by the PES membrane.

The initial configuration of the system composed of 50 TA molecules solvated in pure water and of the system containing the PES membrane and 50 TA molecules solvated in pure water are presented in Figs. 3 and 7, respectively. Figure S5 shows the initial configuration of the other systems with 15 TA molecules.

After the initialization procedure, as described above, 100 ns MD simulations were performed for each of the four systems.

3. Results and discussion

3.1. Tannic acid molecules in water

3.1.1. TA-TA interactions

Tannic acid (TA) self-aggregation is a phenomenon observed experimentally, forming aggregates of several hundred nanometers [31,35]. This phenomenon could be at the origin of membrane fouling. However, the interactions that cause this self-aggregation have never been clearly identified. It is therefore crucial to understand the interactions involved in TA aggregation to better control them. Moreover, a minimal concentration, between 0.5 and 3 g/L according to different studies [34,35], has been shown to be necessary to observe the aggregation of TA molecules. Thus, to study the interactions involved in TA self-aggregation and to account for the effect of TA concentration, two systems were considered, one containing 15 TA molecules (9 g/L) and another one containing 50 TA molecules (30 g/L). In these systems, the number of TA molecules is large enough to study TA-TA interactions and corresponds to concentrations largely sufficient to observe the aggregation, while being significantly below the TA solubility, of 300 g/L in water [66].

Whatever the TA concentration, results presented in Table 1 show that attractive interactions between TA molecules take place, essentially through intermolecular hydrogen bonds (H-bonds) like interactions and intermolecular π-stacking interactions. These interactions are at the origin of the aggregation phenomenon observed between TA molecules. Fig. 3 shows the initial and final configuration of the system composed of

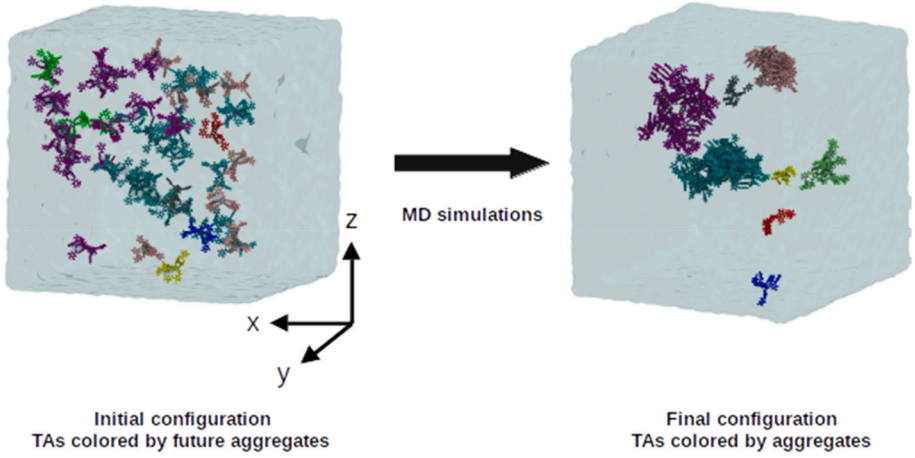

Fig. 3. Representation of the initial and final configuration of the system composed of 50 TA molecules in water (30 g/L). Water is displayed in QuickSurf representation in cyan, and TAs from the same final aggregate are displayed in the same color. (For interpretation of the references to color in this figure legend, the reader is referred to the Web version of this article.)

Table 1
Interactions responsible for TA aggregation for systems composed of 15 or 50 TA molecules in water (9 or 30 g/L), in the presence or absence of a PES membrane. The number of aggregated TAs was determined on the final system configuration, as the number of TAs within 5 Å of another TA molecule. All the interactions were averaged over the number of aggregated TAs. The intermolecular π-stacking interactions were averaged over the last 20 ns. The intermolecular H-bond interactions were averaged over the last 10 ns. The number of O(Alcohol) … H(Alcohol), O(Alcohol) … H(Aromatic), O(Carbonyl) … H(Alcohol) and O(Carbonyl) … H(Aromatic) interactions were counted up to a maximum interaction length of 2.5, 5, 2.5 and 3.5 Å, respectively.

System Composition	Number of aggregated TAs	Number of TA-TA π-Stacking	Number of TA-TA H-bonds			
			O(Alcohol) … H(Alcohol)	O(Alcohol) … H(Aromatic)	O(Carbonyl) … H(Alcohol)	O(Carbonyl) … H(Aromatic)
PES + 15 TAs (9 g/L)	11	1.3	0.2	9.4	0.9	3.0
PES + 50 TAs (30 g/L)	47	1.8	0.3	13.3	0.9	2.5
15 TAs (9 g/L)	14	1.6	0.2	9.6	0.5	2.0
50 TAs (30 g/L)	46	2.2	0.5	16.1	1.1	3.0

50 TAs. More snapshots of the studied systems are displayed in Figure S5.

The interaction between TA molecules was firstly followed by calculating the number of aggregated TAs, considering a distance of 5 Å as the upper limit for aggregation criterion. Table 1 summarizes the final number of aggregated TAs in each system. A description of the formed aggregates (number of TAs per aggregate and associated radius of gyration) is given in Table 2, Table S3 and Figure S6. Fig. 4 shows the evolution of the number of aggregated TAs over time, during the production part of the MD simulation. The construction of the systems involved the random placement of TA molecules, some of them being placed really close to another TA molecule (and so already considered aggregated) in the initial configuration of the system. Moreover, during the initialization procedure (see Materials and methods), the closest TA molecules already started to aggregate, explaining why the number of aggregated TAs does not start from 0 in Fig. 4. Then, after a rapid increase of the number of aggregated TAs during about the first 25 ns of the MD simulation, a plateau is reached around 50 ns. As a result, 14 or 46 TA molecules were aggregated for systems composed of 15 or 50 TAs,

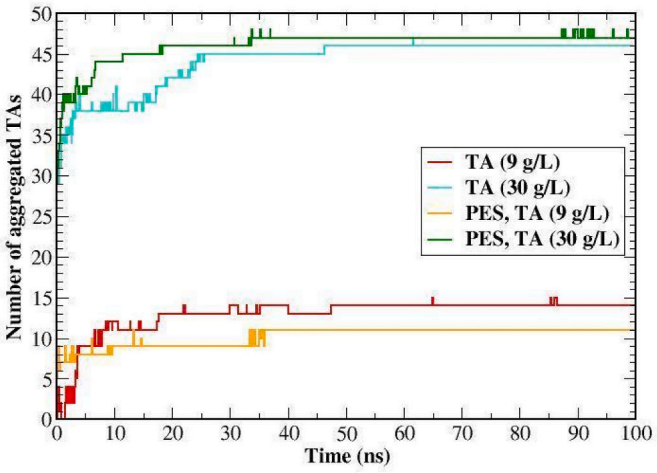

Fig. 4. Evolution of the number of aggregated TAs over time, for systems composed of 15 or 50 TA molecules in water (9 or 30 g/L), in the presence or absence of a PES membrane.

Table 2
Description of each aggregate for systems composed of 15 or 50 TA molecules in water (9 or 30 g/L), in the presence or absence of a PES membrane. The number of TAs per aggregate, the number of adsorbed TAs and the radius of gyration (Å) were determined on the final system configuration. For systems containing a PES membrane, the number of directly adsorbed TAs is also indicated (adsorption criterion: within 5 Å of the PES membrane). Table S3 provides snapshots of each aggregate.

System	Number of aggregate	Aggregate Characteristics		
		Number of TAs per aggregate	Number of adsorbed TAs	Radius of gyration (Å)
PES + 15 TAs (9 g/L)	3	1	1	7.5/7.8/7.9
	1	1	0	8.5
	2	2	2	9.3/13.3
	1	7	3	16.0
PES + 50 TAs (30 g/L)	3	1	1	7.8/8.1/8.1
	1	2	2	9.4
	1	3	3	13.6
	1	4	4	12.1
	1	5	0	13.3
	1	5	4	12.6
	1	7	6	15.9
	1	21	2	30.4
15 TAs (9 g/L)	1	1	–	8.3
	1	2	–	10.5
	2	3	–	10.2/10.5
	1	6	–	14.4
50 TAs (30 g/L)	4	1	–	7.5/7.7/8.1/8.7
	1	3	–	11.7
	1	8	–	15.6
	1	15	–	20
	1	20	–	23.5

respectively, corresponding to more than 90% of TA molecules. These results demonstrate that the aggregation is very favorable. It appears that the trend in the number of aggregated TAs only increases over time and reaches a plateau that corresponds to a state of equilibrium. Moreover, the distribution of the number of TAs by aggregate as a function of time is presented in Figure S7. These results reveal that the formed aggregates exhibit minimal variation after 60 ns, validating the simulation time used as sufficient to observe the aggregation process. Hence, it can be inferred that the formed TA aggregates are stable and stabilize the system.

To better understand this aggregation, the intermolecular TA-TA interactions involved in aggregation were analyzed. For all analyses, classical strong H-bonds (O–H···O) and nonclassical weak H-bonds (C–H···O, also denoted weak interactions) are differentiated, as defined by Karas et al. [67]. Moreover, for strong H-bonds, an angle (α) defined as O–H···O will be considered, where α required to fall within the range of 130–180°; while for weak H-bonds the C–H···O angle must be within the range of 90–180° [68]. Thus, four major intermolecular interactions were identified: two H-bonds (O(Carbonyl) … H(Alcohol) and O (Alcohol) … H(Alcohol)) and two weak interactions (O(Carbonyl) … H (Aromatic) and O(Alcohol) … H(Aromatic)). An overview of the corresponding interactions is presented in Fig. 5, showing an aggregate of 20 TA molecules found in the system composed of 50 TAs. The final number of each type of interaction is reported in Table 1, for the four systems studied. To avoid counting the intramolecular interactions, it was calculated for each TA with respect to all the other TAs. The number of interactions was then averaged over the number of aggregated TAs in

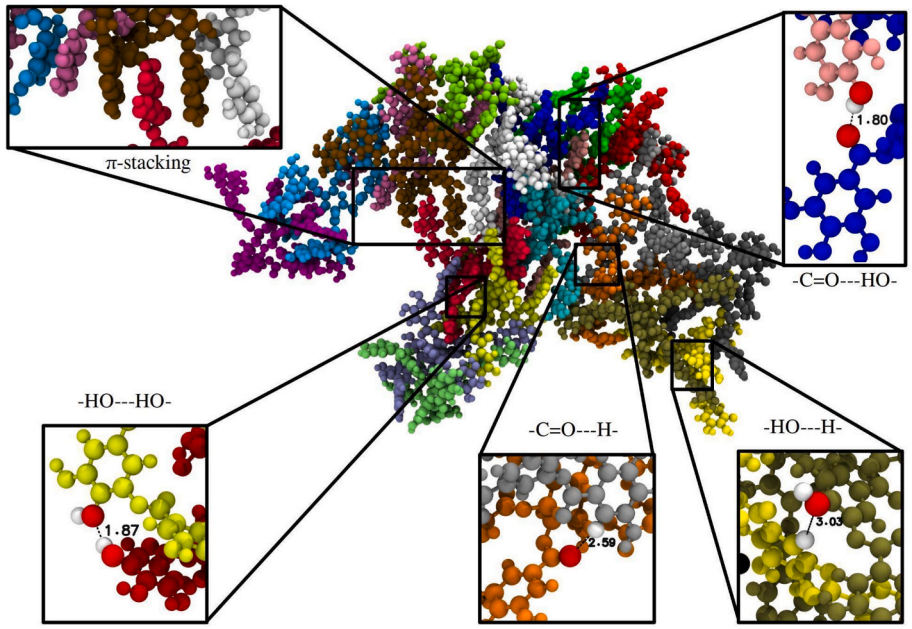

Fig. 5. Snapshot of TA-TA intermolecular interactions (H-bond and π-stacking) found in an aggregate of 20 TA molecules, in the system composed of 50 TA molecules in water (30 g/L). Water is not shown for clarity. The length of the highlighted interactions is given in Å.

the system.

Finally, the Radial Distribution Function (RDF) corresponding to these intermolecular interactions was computed for a better characterization. Only the RDF profile calculated for 50 TAs is shown in Fig. 6, the RDFs for the other systems being qualitatively similar (see Figure S8). According to RDF profiles, both carbonyl and alcohol oxygens formed H-bonds with hydrogen atoms of alcohol groups (Fig. 6, purple and blue line, respectively). These interactions, which occur between 1.5 and 2.5 Å, are the strongest, as expected, with a more probable length of ~1.8 Å. As shown in Table 1, the average number of these H-bonds is similar, with 0.2 O(Alcohol) … H(Alcohol) and 0.5 O(Carbonyl) … H(Alcohol) H-bonds per TA, for the system composed of 15 TAs. The same tendencies are observed for the 50 TA system. Hydrogen atoms from the aromatic ring are also involved in weak interactions (see definition above) with oxygen from carbonyl or alcohol groups (See Fig. 6, orange and pink line, respectively). The first sphere of interaction of the O (Carbonyl) … H(Aromatic) ranges between 2.0 and 3.5 Å, with a maximum peak height at ~2.8 Å. The distance of the O(Alcohol) … H (Aromatic) interaction is more extensive, ranging from 2 to 5 Å, with a maximum at ~3.8 Å. When comparing different interaction strengths, it can be noticed that those involving hydrogen of the alcohol groups were established at shorter distances, representing stronger interactions than those involving an aromatic hydrogen, which is consistent with the more important polarity of O–H bonds compared to C–H bonds. Weak interactions (C–H···O) can occur by two physico-chemical processes, a direct one or an indirect one, mediated by the formation of stronger H-bonds (O–H···O) in the vicinity of aromatic hydrogen. Quantification of these two processes reveals that 74–93% of weak interactions are not mediated by strongest H-bonds (see Figure S9 and Tables S4, S5). In any case, all these interactions, even indirect weak interactions, contribute to the self-aggregation of TA molecules and are all implied in the stability of the aggregates.

TA self-aggregation is also directed by the formation of π-stacking intermolecular interactions. Intermolecular TA-TA π-stacking were defined as the interaction between two aromatic rings close to less than 5 Å (defined by Headen et al. as the upper limit to observe parallel π-stacking [69]), and whose angle between the vectors normal to the rings is smaller than π/12 radians. It is important to note that the number of π-stacking interactions was averaged by the number of aggregated TAs. That is to say that if two TA molecules are connected by

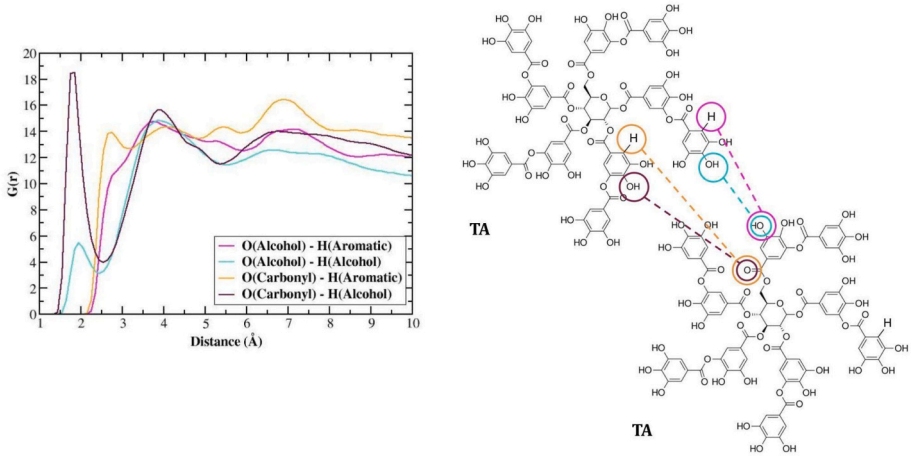

Fig. 6. Radial distribution function characterizing TA-TA intermolecular interactions for the system composed of 50 TA molecules in water (30 g/L).

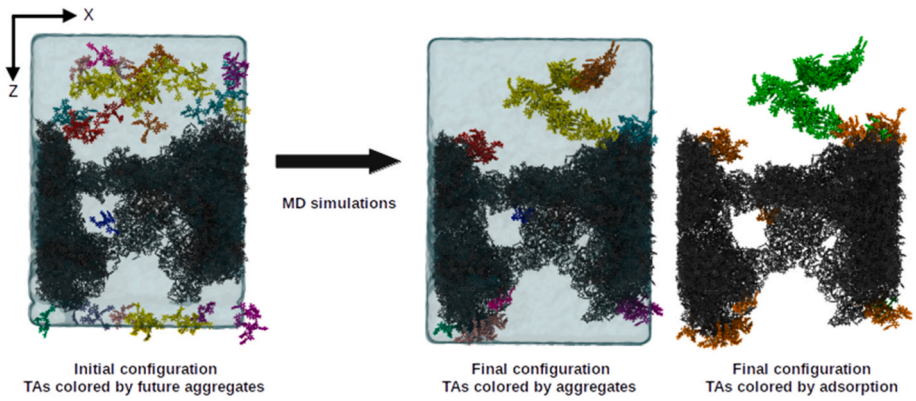

Fig. 7. Representation of the initial and final configuration of the system composed of a PES membrane and 50 TA molecules in water (30 g/L). Water is displayed in QuickSurf representation in cyan. On the left and middle snapshots, TA molecules from the same final aggregate are displayed in the same color. On the right snapshot, TA molecules are colored according to adsorption (adsorption criterion: within 5 Å of the PES membrane; orange: adsorbed, green: not adsorbed). On the right snapshot, water is not shown for clarity. (For interpretation of the references to color in this figure legend, the reader is referred to the Web version of this article.)

two π-stacking interactions, there is on average one π-stacking interaction per TA. But there are therefore two aromatic rings per TA (the double) which is involved in an π-stacking interaction. The same is true for the previously presented H-bond interactions. For the system composed of 15 TAs, there are about 1.6 π-stacking interactions per TA. Considering the case of simple π-stacking (each aromatic ring involved in only one π-stacking interaction), it can be deduced that each TA has 3.2 rings involved in π-stacking. TA has ten aromatic rings, indicating that approximately 32% of the aromatic rings are involved in intermolecular π-stacking interactions. For the 30 g/L system, 44% of the aromatic rings are implied in intermolecular π-stacking interactions. However, the TA-TA π-stacking residence time (Figure S10) exhibits that in fact, during the last 2 ns of simulation, more than 50% of the aromatic rings were involved in these interactions at least 10% of the time, for both systems, revealing that TA-TA π-stacking represents dynamic interactions, made and unmade frequently because of the flexible geometry of TA molecules. Additionally, 21 and 18% of the aromatic rings are involved in intramolecular TA-TA π-stacking, for 9 and 30 g/L systems, respectively.

However, more complex π-stacking structures were observed, involving multiple consecutive aromatic rings stacked together. Fig. 5 shows six aromatic cycles, from five different TA molecules, stacked together. Considering this type of configuration, and that the number of interactions is averaged over the number of aggregated TAs, the total number of aromatic rings involved in π-stacking interactions is therefore less than 32–44%. Nonetheless, this arrangement demonstrates favorable interconnection of the aggregated TAs, supported by the fact that the formed aggregates do not break down during the simulation (Figure S7), which agrees with the very stable character of their aggregation in solution.

3.1.2. *Effect of TA concentration on TA self-aggregation*

As mentioned previously, in both systems studied, the proportion of aggregated TAs is approximately the same at the end of the simulation, i.e., over 90%. However, the number of O(Alcohol) … H(Alcohol) H-bonds per TA increases from 0.2 to 0.5 when the concentration increases from 9 to 30 g/L. The other studied interactions follow the same trend, in particular the number of O(Carbonyl) … H(Alcohol) interactions, which double from 0.5 to 1.1 interactions per TA, with the increase of the concentration (Table 1).

Table 2 gives a description of each aggregate (number of TAs per aggregate and associated radius of gyration) for all the systems studied. It was observed that the largest aggregates formed were composed of 40% of the total number of TA molecules, i.e., 6 and 20 TAs for the 9 and 30 g/L systems, respectively. The formation of larger aggregates in the 30 g/L system may explain the increase in the number of TA-TA interactions observed. Indeed, the greater the number of molecules forming the aggregate, the greater the number of neighboring TAs accessible to form interactions. This allowed the establishment of more intermolecular interactions. In summary, increasing TA concentration correlates with increased aggregate size and number of TA-TA interactions, thus contributing to stronger aggregation.

3.2. *PES membrane and TA molecules*

The adsorption of polyphenols on the surface of PES membranes is a phenomenon that contributes to membrane fouling, a mechanism that is still not clearly understood [30]. The formation of non-covalent interactions between the compounds and the membrane is at the origin of the adsorption; however, no study has yet clearly characterized which interactions are at the origin of the adsorption.

Therefore TA-PES interactions were analyzed to elucidate this phenomenon. For this purpose, two systems composed of a PES membrane and 15 or 50 TAs were studied by molecular dynamics, considering the previous TA concentrations (9 or 30 g/L).

Two main phenomena were observed during these MD simulations. On the one hand, the attractive interactions between TA molecules and the PES membrane, through H-bond and π-stacking interactions is observed; on the other hand, TA self-aggregation still occurs.

3.2.1. *TA-PES interactions*

To study the interactions involved in TA adsorption onto a PES membrane and to account for the effect of TA concentration, two systems were considered, one containing a PES membrane and 15 TA molecules (9 g/L) and another one containing a PES membrane and 50 TA molecules (30 g/L). In these systems, the TA concentrations are largely sufficient to observe the interactions associated with membrane fouling, as supported by a prior experimental study that documented fouling of a pristine PES membrane by a TA solution at a concentration of 10 mg/L [29]. The adsorption of a compound onto a membrane is generally defined by a separation distance between interacting atoms ranging from 4 to 6 Å [42,70]. Here, a threshold of 5 Å was thus considered as a criterion to characterize adsorption phenomenon. Accordingly, adsorption of several TAs on the PES membrane was observed in both simulations. Fig. 7 shows the initial and final configuration of the system composed of a PES membrane and 50 TAs. More snapshots of the studied systems are displayed in Figure S5.

Table 3 summarizes the final number of adsorbed TAs onto the PES membrane, for different TA concentrations (9 or 30 g/L). It is observed that 10 or 24 TA molecules are directly adsorbed for systems composed

Table 3
Interactions responsible for TA adsorption for systems composed of a PES membrane and 15 or 50 TA molecules in water (9 or 30 g/L). The number of adsorbed TAs was determined on the final system configuration, as the number of TAs within 5 Å of the PES membrane. All the interactions were averaged over the number of adsorbed TAs. The π-stacking interactions were averaged over the last 20 ns. The H-bond interactions were averaged over the last 10 ns. The number of H(TA-Alcohol) … O(PES-Sulfonyl), H(TA-Aromatic) … O(PES-Sulfonyl), O(TA-Carbonyl) … H(PES-Aromatic) and O(TA-Alcohol) … H(PES-Aromatic) interactions were counted up to a maximum interaction length of 2.5, 3.5, 3.5 and 5 Å, respectively.

System Composition	Number of adsorbed TAs	Number of TA-PES π-Stacking	Number of TA-PES H-bonds			
			H(TA-Alcohol) … O(PES-Sulfonyl)	H(TA-Aromatic) … O(PES-Sulfonyl)	O(TA-Carbonyl)… H(PES-Aromatic)	O(TA-Alcohol) … H(PES-Aromatic)
PES + 15 TAs (9 g/L)	10	1.1	0.7	2.0	3.3	34.6
PES + 50 TAs (30 g/L)	24	0.8	0.5	1.3	2.6	22.0

of 15 or 50 TAs, corresponding to 67 or 48% of the TA molecules present in the system, respectively. This reflects an affinity between TA and the PES membrane.

Moreover, individual TA molecules as well as aggregates are adsorbed onto the membrane (see Table 2). Indirect adsorption will be defined as a TA molecule not directly adsorbed onto the membrane but belonging to an aggregate adsorbed onto the membrane. For instance, in the system composed of a PES and 50 TAs, an aggregate of 21 TAs is adsorbed onto the membrane (colored in yellow in the middle snapshot of Fig. 7). Only 2 TA molecules of this aggregate are within 5 Å of the membrane (colored in orange in the right snapshot of Fig. 7), and so considered directly adsorbed. The remaining 19 TAs of this yellow aggregate are more than 5 Å away from the membrane, but they can be considered indirectly adsorbed, because they are part of an aggregate adsorbed onto the membrane. If one considers the total of directly and indirectly adsorbed TA molecules, not 24 but 45 TA molecules are adsorbed, increasing the number of adsorbed TA molecules from 48 to 90%; with only one aggregate composed of 5 TA molecules totally free in solution. For the system composed of a PES and 15 TAs, considering both direct and indirect adsorption leads to an increase in the number of aggregated TAs from 67 to 93%.

However, the observed results must be put into perspective with the simulation times which may be too short to observe the whole adsorption phenomenon. For example, as presented in Fig. 7, one TA aggregate (displayed in yellow in the middle snapshot) is only adsorbed through a few molecules of TA and does not maximize its contact area with the PES. However, Figure S11 shows the minimum distance between two atoms of TA and PES for each TA molecule at different simulation times. It can be observed that some of the initially furthest TA molecules from the membrane were adsorbed at the end of the 100 ns simulation. It is safe to conclude that the simulation times used (100 ns) are long enough to allow TAs to diffuse into the medium and finally adsorb onto the membrane, whatever the initial distance between the TA molecule and the PES membrane. Moreover, the TA-PES distance exhibits minimal variation between 50 and 100 ns for most of the TA molecules, which provides reassurance that the simulated time is adequate for the adsorption process to reach a state of equilibrium. Nonetheless, the simulation time may be too short to allow the observation of a larger adsorption phenomenon of some large aggregates, which would therefore have a longer diffusion time. Finally, Fig. 8 describes the evolution of the number of adsorbed TAs over time, reaching a plateau around 60 ns, suggesting again that 100 ns is sufficient to reach a state of equilibrium. It also supports that the number of adsorbed TAs only increases over time, approving the fact that an adsorbed TAs no longer desorbs based on the simulation times used. This confirms the stable character, during the simulation, of the TA-PES interactions leading to adsorption.

During adsorption, π-stacking interactions and four main TA-PES interactions were identified: one strong H-bond (H(TA-Alcohol) … O (PES-Sulfonyl)), and three weak interactions (O(TA-Carbonyl) … H (PES-Aromatic), H(TA-Aromatic) … O(PES-Sulfonyl) and O(TA-Alcohol) … H(PES-Aromatic)). The final number of each type of

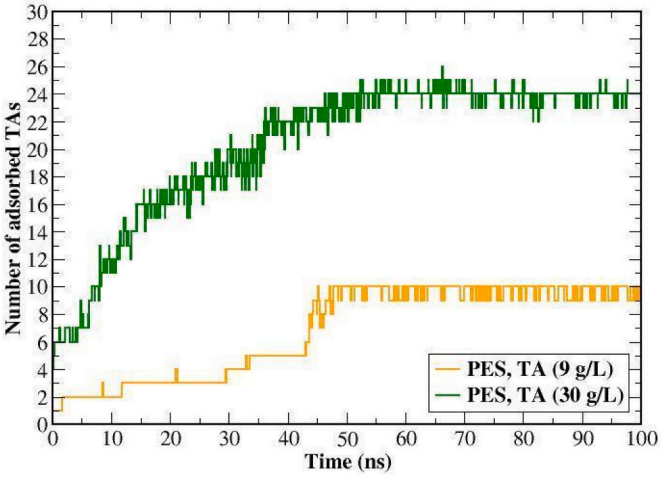

Fig. 8. Evolution of the number of adsorbed TAs over time, for the systems composed of a PES membrane and 15 or 50 TA molecules in water (9 or 30 g/L).

interaction is reported in Table 3, as a function of TA concentration.

To study these interactions, the TA-PES RDF was also calculated. Fig. 9 shows the TA-PES RDF for the system composed of a PES membrane and 50 TAs (30 g/L). Figure S12 shows the similar TA-PES RDF for the system composed of a PES membrane and 15 TAs. It appears that the H-bond interaction between the alcohol hydrogen of TA and the oxygen from the sulfonyl group of PES (H(TA-Alcohol) … O(PES-Sulfonyl)) is the strongest, as expected, with a first interaction sphere at distances ranging from 1.5 to 2.5 Å (most probable interaction length at ~1.8 Å). The two other weak interactions, between aromatic hydrogen atoms of TA and the sulfonyl group of PES (H(TA-Aromatic) … O(PES-Sulfonyl)), and between the carbonyl group of TA and the aromatic hydrogen atoms of PES (O(TA-Carbonyl) … H(PES-Aromatic)) occur between 2.0 and 3.5 Å, with an average interaction length of ~2.8 Å. These interactions correspond therefore to weaker interactions, compared to the H(TA-Alcohol) … O(PES-Sulfonyl) H-bond. Finally, a weak O(TA-Alcohol) … H(PES-Aromatic) interaction was found between the oxygen groups of TA and the aromatic hydrogen atoms of PES, ranging from 2.0 to 5.0 Å with a most probable interaction length at ~3.5 Å.

As reported in Table 3, H(TA-Alcohol) … O(PES-Sulfonyl) strong interactions are less abundant than H(TA-Aromatic) … O(PES-Sulfonyl) weak interactions, respectively 0.7 and 2.0 interactions on average per adsorbed TA, for the 9 g/L system. There are way more weak interactions involving aromatic hydrogen from the PES. In fact, there are 34.6 O(TA-Alcohol) … H(PES-Aromatic) interactions, up to 5.0 Å; and there are 3.3 O(TA-Carbonyl) … H(PES-Aromatic) interactions, up to 3.5 Å, per adsorbed TA, involved in the adsorption of TAs onto PES. There are 10 O(Carbonyl) groups in a TA molecule, which means that, on average, 33% of the oxygens from the carbonyl groups of adsorbed TAs interact with PES, at 9 g/L and 26% at 30 g/L. As previously

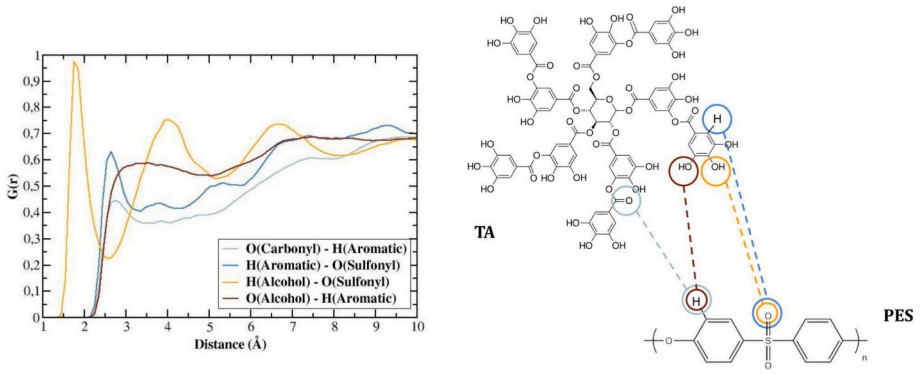

Fig. 9. Radial distribution function characterizing TA-PES interactions, for the system composed of a PES membrane and 15 TA molecules in water (9 g/L).

mentioned for TA-TA interactions, weak interactions can result from a direct or an indirect process, mediated by the formation of stronger H-bonds nearby. Tables S6, S7 and S8 show that 75–91% of TA-PES weak interactions are not mediated by strongest H-bonds. In any case, all these interactions, even indirect weak interactions, contribute to the stability of the adsorbed TA molecules.

Parallel to the formation of these peculiar interactions, π-stacking interactions were identified between TA and PES. TA-PES π-stacking were defined as the interaction between two aromatic rings close to less than 5 Å, and whose angle between the vectors normal to the rings is smaller than π/12 radians. It appears that these π-stacking interactions are less numerous than the H-bond interactions, with approximately 1.1 and 0.8 TA-PES π-stacking interactions per adsorbed TA, for 9 and 30 g/L systems, respectively (see Table 3).

3.2.2. TA self-aggregation vs adsorption

In the last part, the study focused on evaluating the impact of the membrane on TA-TA interactions, and thus on the TA aggregation. Table 1 summarizes the final number of aggregated TAs in each system, as well as the final number of π-stacking and other interactions, for systems composed of a PES membrane and TAs at 9 or 30 g/L and for systems only composed of TAs at 9 or 30 g/L, allowing to study the impact of PES on TA aggregation.

In the system composed of a PES membrane and 50 TAs, a final number of 47 aggregated TAs is obtained, similar to the 46 aggregated TAs found in the 50 TA system. While not impacting the final number of aggregated TAs, the addition of the PES membrane is however associated with a slight decrease in intermolecular TA-TA interactions involved in TA self-aggregation. In the 30 g/L systems, when the PES membrane was added to the system, the number of TA-TA H-bond interactions decrease from 0.5 to 0.3, 16.1 to 13.3 and 3.0 to 2.5 for O (Alcohol) … H(Alcohol), O(Alcohol) … H(Aromatic) and O(Carbonyl) … H(Aromatic) interactions, respectively. With regard to π-stacking interactions, the addition of the PES membrane leads to a decrease from 1.6 to 1.3 TA-TA interactions per TA, for systems composed of 15 TAs (9 g/L).

It is interesting to notice that the same TA atoms (i.e., O(Carbonyl), H (Aromatic), and H(Alcohol)) are involved in TA-PES and TA-TA interactions. It explains the decrease in the number of TA-TA H-bond interactions in the presence of PES due to competition between these interactions. Indeed, when TA adsorbs onto the membrane, some of the atoms are involved in TA-PES interactions and thus are not available for TA-TA interactions. The same applies to TA-TA and TA-PES π-stacking, which both involve aromatic rings from TA. Indeed, the TA-TA π-stacking interactions, appearing during aggregation, also decreased from 2.2 to 1.8 when the membrane was added to the 30 g/L system (see Table 1).

The mechanism of PES membrane fouling by polyphenols remains poorly understood. One of the proposed mechanisms is the rapid adsorption of TA on the membrane, followed by aggregation of TAs at the level of the pores, which can lead to pore blocking [31]. The present results highlight self-aggregation of TAs and their adsorption onto the PES membrane. Thus, a comparison of the kinetics of these two phenomena, aggregation and adsorption, could help to understand how the fouling mechanism is set up. Figs. 8 and 10, which respectively described the number of adsorbed TAs over time and the mean number of TAs per aggregate over time, show that the aggregation and the adsorption occurred in parallel. Indeed, both phenomena increased progressively during the simulation before reaching a plateau around 60 ns of simulation. TA-PES and intermolecular TA-TA interactions gradually consolidate in parallel. Thus, the kinetics of aggregation and adsorption are sufficiently similar for the concomitant formation of the two observed phenomena.

Another interesting aspect is that there are 1.1 and 0.8 TA-PES π-stacking interactions per adsorbed TA (for the 9 and 30 g/L systems, respectively), corresponding to about 10% of the aromatic rings of the TAs (Table 3). These TA-PES interactions are significantly less important than TA-TA π-stacking interactions which involve 32–44% of the aromatic rings. This difference could come from the PES membrane geometry, which is much less flexible than TA geometry, the spatial orientation of the rings favoring π-stacking being easier for TA molecules to reach.

In the simulations, TAs were neither aggregated nor adsorbed in the starting configuration. It has been shown that TA-TA and TA-PES interactions are formed in parallel, and that the establishment of TA-PES interactions reduces the number of TA-TA interactions. Accordingly, it

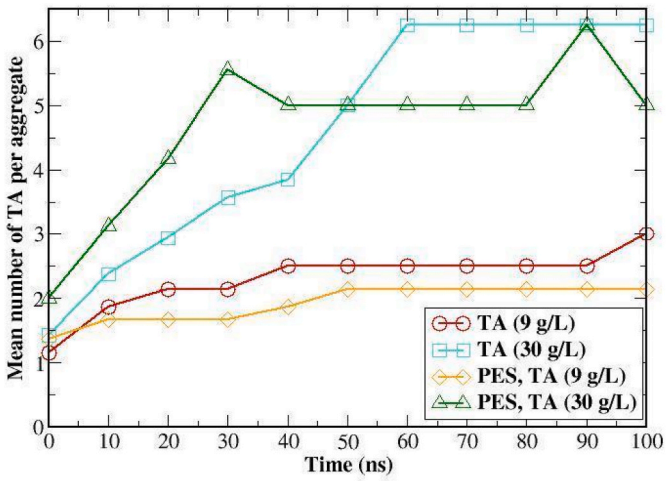

Fig. 10. Evolution of the mean number of TAs per aggregate over time, for the systems composed of 15 or 50 TA molecules in water (9 or 30 g/L), in the presence or absence of the PES membrane.

would be interesting to investigate the impact of the addition of the PES membrane on a system in which the TAs are already aggregated.

3.2.3. TA and PES solvation

In the MD simulations, interactions between water molecules and TA were observed. Specifically, some water molecules were found trapped within the aggregates, presumably contributing to the aggregate's structure and stability. Moreover, water molecules bridging some hydrophilic groups (alcohol and carbonyl) of different TAs within an aggregate were also observed. It is essential to note that our focus was primarily on direct TA-TA interactions and that these indirect TA-TA interactions mediated by water molecules were not extensively explored. As a result, the number of TA-TA interactions may have been underestimated by not taking into account the water mediated interactions. However, no water molecules were observed intercalating between the aromatic cycles engaged in TA-TA π-stacking interactions, as expected regarding the hydrophobicity of these functional groups.

Further investigations have been made about the interactions of TAs with water molecules. Table S9 details the difference of the number of water molecules within 3.5 Å of the TAs at the beginning and end of the MD simulations. Notably, in the system composed of a PES membrane and 50 TAs, the number of water molecules around TAs decreases by 34% during the simulation. No significant difference is observed between TAs that are only aggregated, only adsorbed, and both adsorbed and aggregated, with a reduction of the number of water molecules of 30%, 20%, and 32%, respectively. Interestingly, for the system composed of 50 TAs, it is observed that for the TAs that are neither aggregated nor adsorbed there is still a decrease of 17% in solvating water molecules, suggesting a modification in TA conformation during the MD simulation even without direct TA-TA or TA-PES interactions.

To deepen the understanding of the observed reduction of TA solvation, Fig. 11 shows the TA-water RDFs for the system composed of a PES membrane and 50 TAs (30 g/L), with solid lines for the first 10 ns and dashed lines for the last 10 ns of the simulation, aiming at studying the evolution of TA solvation. The RDFs for the other systems being qualitatively similar are not presented here (see Figure S13). The aromatic cycles of TA do not interact strongly with water (Fig. 11a). Specifically, the first hydration shell of aromatic carbon of TA has a most probable length of ~4.2 Å, corresponding to the C(TA-Aromatic) … H (Water) interaction, indicating minimal hydration of the aromatic cycles. Similarly, the H(TA-Aromatic) … O(Water) interaction indicates that the hydration sphere of the aromatic hydrogen of TA ranges from 2 to 4 Å with a most probable distance length of ~2.8 Å, signifying a relatively weak interaction. Additionally, the density of interactions between water and TA aromatic atoms decreases towards the end of the simulation, suggesting that, during TA adsorption and aggregation, the hydrophobic parts of TA effectively shielded themselves from water. In contrast, alcohol groups displayed stronger interactions with water (Fig. 11b). A O(TA-Alcohol) … H(Water) interaction is observed at distances ranging from 1.5 to 2.5 Å, corresponding to a strong interaction with a most probable length of ~1.9 Å. Moreover, hydrogen from the alcohol group of TA interacts strongly with the oxygen of water, at a short distance of ~1.8 Å. A slight decrease in the density of water molecules around the atoms of the alcohol groups by the end of the simulation is observed. It is attributed to some alcohol groups being located inside the aggregates and not exposed to the solvent. However, this diminution was markedly less pronounced than the substantial drop observed for atoms of the aromatic groups. This indicates that hydration of the more hydrophilic groups (alcohol groups) is less affected by aggregation and adsorption than hydrophobic groups of TA. These results suggest that TA aggregation and adsorption is favorable in water. Indeed, the overall TA solvation decreases as hydrophobic groups engage in π-stacking interactions to minimize water interaction, while the hydrophilic groups located at the TA molecule's periphery remain exposed to water.

Regarding PES-water interactions, a similar trend is observed (Figure S14). A reduction of the solvation of the PES membrane is observed (Table S9), in line with the hydrophobic character of the membrane, benefiting from TA adsorption to enhance TA-PES interactions and minimize PES-water interactions. See the discussion on Figure S14 for a detailed characterization of PES-water interactions.

4. Conclusions

In summary, all-atom MD simulations were conducted to characterize the interactions involved in the fouling process during the filtration of tannic acid (TA) by a polyethersulfone (PES) membrane. A porous PES membrane with pore size ranging from 3 to 13 nm, in the range of the UF membranes, was modeled. The PES and TA model were validated by the good reproduction of experimental IR spectra from MD simulations, as well as membrane density and surface porosity. Four systems, containing 15 or 50 TA molecules, corresponding to a concentration of 9 or 30 g/L, respectively, were studied in the presence or the absence of a PES membrane.

TA self-aggregation was investigated and up to 90% of TA molecules were aggregated, revealing the very stable character of the aggregation, according to previous experimental observations. Four main H-bond interactions were associated to the aggregation, involving the hydrogen atoms from the alcohol and aromatic groups as donor and the oxygens from the alcohol and carbonyl groups as acceptor. Interactions forming via the hydrogen from the alcohol groups, as H-bond donors, were the strongest, in accordance with the higher polarity of the O–H bonds compared to C–H bonds. Intermolecular TA-TA π-stacking interactions were also identified as key interactions controlling the aggregation phenomenon.

The adsorption of TA onto the PES membrane was observed in the simulations. H-bond interaction between the oxygen from the sulfonyl group of PES and hydrogen from the alcohol group of the TA was the strongest one. However, more than four times as many interactions were found between the carbonyl group of the TA and aromatic hydrogen of

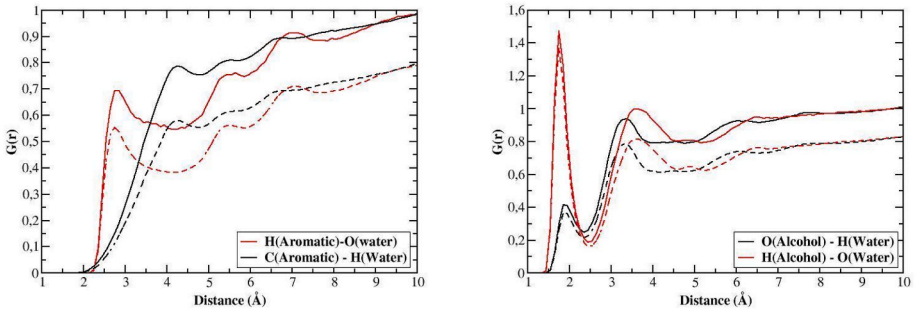

Fig. 11. Radial distribution function characterizing TA-water interactions, for the system composed of a PES membrane and 50 TA molecules in water (30 g/L). Solid lines correspond to the RDF calculated during the first 10 ns of the simulation and dashed lines to the RDF calculated from the last 10 ns of the simulation. RDFs are presented for water interacting with different functional groups of TA: a) Aromatic rings and b) Alcohol.

the PES, implying that the adsorption occurs not only through the sulfonyl group of the membrane but also through weaker interactions involving aromatic rings of the PES. Moreover, TA-PES π-stacking interactions were also an important contribution to the adsorption.

The adsorption and the self-aggregation of TA molecules are two phenomena that occurred in parallel and are in competition as the same groups of atoms are implied in TA-TA and TA-PES interactions. Then TA-PES interactions should be regulated by controlling the TA aggregation. Moreover, ~50% of the TAs were directly adsorbed while an additional 40% was indirectly adsorbed onto the surface through aggregation, meaning that, even if there are only a few TA molecules free in solutions, not all the TAs are directly interacting with the PES surface. These results suggest that both adsorptive fouling and the formation of a cake layer composed of aggregated TAs should be at the origin of the fouling of the membrane. Comparing the strength of TA-PES and TA-TA interactions would represent interesting future investigations to determine which of the adsorptive fouling or cake layer formation is associated with more severe fouling.

Finally, higher TA concentration (30 g/L) leads to the formation of bigger aggregates and more intermolecular TA-TA interactions, suggesting the formation of more strongly interacting aggregates, harder to break. As the aggregation of TAs could lead to fouling by forming large particles leading to complete or partial pore blocking, as well as promoting the formation of a cake layer, the control of the TA concentration may help control fouling.

CRediT authorship contribution statement

Marie Certiat: Writing – review & editing, Writing – original draft, Visualization, Validation, Software, Project administration, Methodology, Formal analysis, Data curation, Conceptualization. **Johanne Teychené:** Writing – review & editing, Validation, Supervision, Resources, Project administration, Methodology, Investigation, Funding acquisition, Formal analysis, Data curation, Conceptualization. **Christelle Guigui:** Writing – review & editing, Supervision, Funding acquisition, Conceptualization. **Stéphanie Laborie:** Writing – review & editing, Supervision, Funding acquisition, Conceptualization. **Franck Jolibois:** Writing – review & editing, Validation, Supervision, Software, Resources, Project administration, Methodology, Investigation, Funding acquisition, Data curation, Conceptualization.

Declaration of competing interest

The authors declare that they have no known competing financial interests or personal relationships that could have appeared to influence the work reported in this paper.

Data availability

Data will be made available on request.

Acknowledgments

M.C. was a recipient of a PhD scholarship from INSA Toulouse. This work was granted access to the HPC resources of CALMIP supercomputing center under the allocation p0758 and of IDRIS supercomputing center under the allocation A0060810816 made by GENCI.

Appendix A. Supplementary data

Supplementary data to this article can be found online at https://doi.org/10.1016/j.memsci.2024.122570.

References

[1] V. Sorrenti, I. Burò, V. Consoli, L. Vanella, Recent advances in health benefits of bioactive compounds from food wastes and by-products: biochemical aspects, Int. J. Mol. Sci. 24 (2023) 2019, https://doi.org/10.3390/ijms24032019.
[2] A. Rana, M. Samtiya, T. Dhewa, V. Mishra, R.E. Aluko, Health benefits of polyphenols: a concise review, J. Food Biochem. 46 (2022), https://doi.org/10.1111/jfbc.14264.
[3] A. Pizzi, Tannins medical/pharmacological and related applications: a critical review, Sustain. Chem. Pharm. 22 (2021) 100481, https://doi.org/10.1016/j.scp.2021.100481.
[4] K. Sharma, V. Kumar, J. Kaur, B. Tanwar, A. Goyal, R. Sharma, Y. Gat, A. Kumar, Health effects, sources, utilization and safety of tannins: a critical review, Toxin Rev. 40 (2021) 432–444, https://doi.org/10.1080/15569543.2019.1662813.
[5] B. Kaczmarek, Tannic acid with antiviral and antibacterial activity as A promising component of biomaterials—a minireview, Materials 13 (2020) 3224, https://doi.org/10.3390/ma13143224.
[6] A. Sridhar, M. Ponnuchamy, P.S. Kumar, A. Kapoor, D.-V.N. Vo, S. Prabhakar, Techniques and modeling of polyphenol extraction from food: a review, Environ. Chem. Lett. 19 (2021) 3409–3443, https://doi.org/10.1007/s10311-021-01217-8.
[7] O.R. Alara, N.H. Abdurahman, C.I. Ukaegbu, Extraction of phenolic compounds: a review, Curr. Res. Food Sci. 4 (2021) 200–214, https://doi.org/10.1016/j.crfs.2021.03.011.
[8] P. Tapia-Quirós, M.F. Montenegro-Landívar, M. Reig, X. Vecino, J. Saurina, M. Granados, J.L. Cortina, Integration of membrane processes for the recovery and separation of polyphenols from winery and olive mill wastes using green solvent-based processing, J. Environ. Manag. 307 (2022) 114555, https://doi.org/10.1016/j.jenvman.2022.114555.
[9] A. Cassano, C. Conidi, R. Ruby-Figueroa, R. Castro-Muñoz, Nanofiltration and tight ultrafiltration membranes for the recovery of polyphenols from agro-food by-products, Int. J. Mol. Sci. 19 (2018) 351, https://doi.org/10.3390/ijms19020351.
[10] J.A.A. Mejia, A. Ricci, A.S. Figueiredo, A. Versari, A. Cassano, M.N. De Pinho, G. P. Parpinello, Membrane-based operations for the fractionation of polyphenols and polysaccharides from winery sludges, Food Bioprocess Technol. 15 (2022) 933–948, https://doi.org/10.1007/s11947-022-02795-3.
[11] P.R. Pinto, I.F. Mota, C.M. Pereira, A.M. Ribeiro, J.M. Loureiro, A.E. Rodrigues, Separation and recovery of polyphenols and carbohydrates from Eucalyptus bark extract by ultrafiltration/diafiltration and adsorption processes, Sep. Purif. Technol. 183 (2017) 96–105, https://doi.org/10.1016/j.seppur.2017.04.003.
[12] M. El Batouti, N.F. Alharby, M.M. Elewa, Review of new approaches for fouling mitigation in membrane separation processes in water treatment applications, Separations 9 (2021) 1, https://doi.org/10.3390/separations9010001.
[13] C. Lu, Y. Bao, J.-Y. Huang, Fouling in membrane filtration for juice processing, Curr. Opin. Food Sci. 42 (2021) 76–85, https://doi.org/10.1016/j.cofs.2021.05.004.
[14] X. Shi, G. Tal, N.P. Hankins, V. Gitis, Fouling and cleaning of ultrafiltration membranes: a review, J. Water Process Eng. 1 (2014) 121–138, https://doi.org/10.1016/j.jwpe.2014.04.003.
[15] N. Hilal, O.O. Ogunbiyi, N.J. Miles, R. Nigmatullin, Methods employed for control of fouling in MF and UF membranes: a comprehensive review, Separ. Sci. Technol. 40 (2005) 1957–2005, https://doi.org/10.1081/SS-200068409.
[16] D.M. Nisticò, A. Piro, D. Oliva, V. Osso, S. Mazzuca, F.A. Fagà, R. Morelli, C. Conidi, A. Figoli, A. Cassano, A combination of aqueous extraction and ultrafiltration for the purification of phycocyanin from arthrospira maxima, Microorganisms 10 (2022) 308, https://doi.org/10.3390/microorganisms10020308.
[17] C. Zhao, J. Xue, F. Ran, S. Sun, Modification of polyethersulfone membranes – a review of methods, Prog. Mater. Sci. 58 (2013) 76–150, https://doi.org/10.1016/j.pmatsci.2012.07.002.
[18] M.T. Tsehaye, S. Velizarov, B. Van Der Bruggen, Stability of polyethersulfone membranes to oxidative agents: a review, Polym. Degrad. Stabil. 157 (2018) 15–33, https://doi.org/10.1016/j.polymdegradstab.2018.09.004.
[19] H. Susanto, Y. Feng, M. Ulbricht, Fouling behavior of aqueous solutions of polyphenolic compounds during ultrafiltration, J. Food Eng. 91 (2009) 333–340, https://doi.org/10.1016/j.jfoodeng.2008.09.011.
[20] M. Ulbricht, W. Ansorge, I. Danielzik, M. König, O. Schuster, Fouling in microfiltration of wine: the influence of the membrane polymer on adsorption of polyphenols and polysaccharides, Sep. Purif. Technol. 68 (2009) 335–342, https://doi.org/10.1016/j.seppur.2009.06.004.
[21] A. Cassano, C. Conidi, E. Drioli, Comparison of the performance of UF membranes in olive mill wastewaters treatment, Water Res. 45 (2011) 3197–3204, https://doi.org/10.1016/j.watres.2011.03.041.
[22] M. Loginov, N. Boussetta, N. Lebovka, E. Vorobiev, Separation of polyphenols and proteins from flaxseed hull extracts by coagulation and ultrafiltration, J. Membr. Sci. 442 (2013) 177–186, https://doi.org/10.1016/j.memsci.2013.04.036.
[23] C. Russo, A new membrane process for the selective fractionation and total recovery of polyphenols, water and organic substances from vegetation waters (VW), J. Membr. Sci. 288 (2007) 239–246, https://doi.org/10.1016/j.memsci.2006.11.020.
[24] L.D.S. Sousa, B.V. Cabral, G.S. Madrona, V.L. Cardoso, M.H.M. Reis, Purification of polyphenols from green tea leaves by ultrasound assisted ultrafiltration process, Sep. Purif. Technol. 168 (2016) 188–198, https://doi.org/10.1016/j.seppur.2016.05.029.
[25] J.L. Acero, F.J. Benítez, I. Leal, F.J. Real, Removal of phenolic compounds in water by ultrafiltration membrane treatments, J. Environ. Sci. Health, Part A 40 (2005) 1585–1603, https://doi.org/10.1081/ESE-200060651.

[26] T.K. Manios, D. Mattia, M.R. Bird, Fouling of polyethersulphone ultrafiltration membranes during the decaffeination of ground coffee brews, Food Bioprod. Process. 136 (2022) 14–23, https://doi.org/10.1016/j.fbp.2022.09.005.
[27] M. Cifuentes-Cabezas, C. Carbonell-Alcaina, M.C. Vincent-Vela, J.A. Mendoza-Roca, S. Álvarez-Blanco, Comparison of different ultrafiltration membranes as first step for the recovery of phenolic compounds from olive-oil washing wastewater, Process Saf. Environ. Protect. 149 (2021) 724–734, https://doi.org/10.1016/j.psep.2021.03.035.
[28] C.M. Sánchez-Arévalo, A. Pérez García-Serrano, M.C. Vincent-Vela, S. Álvarez-Blanco, Combining ultrafiltration and nanofiltration to obtain a concentrated extract of purified polyphenols from wet olive pomace, Membranes 13 (2023) 119, https://doi.org/10.3390/membranes13020119.
[29] K.H. Chu, Y. Huang, M. Yu, N. Her, J.R.V. Flora, C.M. Park, S. Kim, J. Cho, Y. Yoon, Evaluation of humic acid and tannic acid fouling in graphene oxide-coated ultrafiltration membranes, ACS Appl. Mater. Interfaces 8 (2016) 22270–22279, https://doi.org/10.1021/acsami.6b08020.
[30] M. Cai, Y. Lv, S. Luo, Y. Liu, P. Sun, Fouling behavior of polyphenols during model juice ultrafiltration: effect of membrane properties, Food Bioprocess Technol. 11 (2018) 1787–1793, https://doi.org/10.1007/s11947-018-2110-9.
[31] Y. El Rayess, C. Albasi, P. Bacchin, P. Taillandier, M. Mietton-Peuchot, A. Devatine, Analysis of membrane fouling during cross-flow microfiltration of wine, Innov. Food Sci. Emerg. Technol. 16 (2012) 398–408, https://doi.org/10.1016/j.ifset.2012.09.002.
[32] C. Poncet-Legrand, D. Cartalade, J.-L. Putaux, V. Cheynier, A. Vernhet, Flavan-3-ol aggregation in model ethanolic solutions: incidence of polyphenol structure, concentration, ethanol content, and ionic strength, Langmuir 19 (2003) 10563–10572, https://doi.org/10.1021/la034927z.
[33] A.A. Watrelot, M.P. Day, A. Schulkin, R.J. Falconer, P. Smith, A.L. Waterhouse, K. A. Bindon, Oxygen exposure during red wine fermentation modifies tannin reactivity with poly-l-proline, Food Chem. 297 (2019) 124923, https://doi.org/10.1016/j.foodchem.2019.05.197.
[34] V. Riou, A. Vernhet, T. Doco, M. Moutounet, Aggregation of grape seed tannins in model wineÐeffect of wine polysaccharides, Food Hydrocolloids 16 (2002) 17–23, https://doi.org/10.1016/S0268-005X(01)00034-0.
[35] S. Dultz, R. Mikutta, S.N.M. Kara, S.K. Woche, G. Guggenberger, Effects of solution chemistry on conformation of self-aggregated tannic acid revealed by laser light scattering, Sci. Total Environ. 754 (2021) 142119, https://doi.org/10.1016/j.scitotenv.2020.142119.
[36] M. Ościwieja, Z. Adamczyk, M. Morga, Adsorption of tannic acid on polyelectrolyte monolayers determined in situ by streaming potential measurements, J. Colloid Interface Sci. 438 (2015) 249–258, https://doi.org/10.1016/j.jcis.2014.09.071.
[37] A. Mollahosseini, A. Abdelrasoul, Molecular dynamics simulation for membrane separation and porous materials: a current state of art review, J. Mol. Graph. Model. 107 (2021) 107947, https://doi.org/10.1016/j.jmgm.2021.107947.
[38] Y. Ma, J.W. Chew, Investigation of membrane fouling phenomenon using molecular dynamics simulations: a review, J. Membr. Sci. 661 (2022) 120874, https://doi.org/10.1016/j.memsci.2022.120874.
[39] A. Cassano, G. De Luca, C. Conidi, E. Drioli, Effect of polyphenols-membrane interactions on the performance of membrane-based processes, A review, Coord. Chem. Rev. 351 (2017) 45–75, https://doi.org/10.1016/j.ccr.2017.06.013.
[40] W.-Y. Ahn, A.G. Kalinichev, M.M. Clark, Effects of background cations on the fouling of polyethersulfone membranes by natural organic matter: experimental and molecular modeling study, J. Membr. Sci. 309 (2008) 128–140, https://doi.org/10.1016/j.memsci.2007.10.023.
[41] K. Arandia, N.K. Karna, T. Mattsson, A. Larsson, H. Theliander, Fouling characteristics of microcrystalline cellulose during cross-flow microfiltration: insights from fluid dynamic gauging and molecular dynamics simulations, J. Membr. Sci. 669 (2023) 121272, https://doi.org/10.1016/j.memsci.2022.121272.
[42] T. Virtanen, P. Parkkila, A. Koivuniemi, J. Lahti, T. Viitala, M. Kallioinen, M. Mänttäri, A. Bunker, Characterization of membrane–foulant interactions with novel combination of Raman spectroscopy, surface plasmon resonance and molecular dynamics simulation, Sep. Purif. Technol. 205 (2018) 263–272, https://doi.org/10.1016/j.seppur.2018.05.050.
[43] J.C. Phillips, D.J. Hardy, J.D.C. Maia, J.E. Stone, J.V. Ribeiro, R.C. Bernardi, R. Buch, G. Fiorin, J. Hénin, W. Jiang, R. McGreevy, M.C.R. Melo, B.K. Radak, R. D. Skeel, A. Singharoy, Y. Wang, B. Roux, A. Aksimentiev, Z. Luthey-Schulten, L. V. Kalé, K. Schulten, C. Chipot, E. Tajkhorshid, Scalable molecular dynamics on CPU and GPU architectures with NAMD, J. Chem. Phys. 153 (2020) 044130, https://doi.org/10.1063/5.0014475.
[44] J. Wang, R.M. Wolf, J.W. Caldwell, P.A. Kollman, D.A. Case, Development and testing of a general amber force field, J. Comput. Chem. 25 (2004) 1157–1174, https://doi.org/10.1002/jcc.20035.
[45] J. Wang, W. Wang, P.A. Kollman, D.A. Case, Automatic atom type and bond type perception in molecular mechanical calculations, J. Mol. Graph. Model. 25 (2006) 247–260, https://doi.org/10.1016/j.jmgm.2005.12.005.
[46] Gaussian 09, Revision A.02, M. J. Frisch, G. W. Trucks, H. B. Schlegel, G. E. Scuseria, M. A. Robb, J. R. Cheeseman, G. Scalmani, V. Barone, G. A. Petersson, H. Nakatsuji, X. Li, M. Caricato, A. Marenich, J. Bloino, B. G. Janesko, R. Gomperts, B. Mennucci, H. P. Hratchian, J. V. Ortiz, A. F. Izmaylov, J. L. Sonnenberg, D. Williams-Young, F. Ding, F. Lipparini, F. Egidi, J. Goings, B. Peng, A. Petrone, T. Henderson, D. Ranasinghe, V. G. Zakrzewski, J. Gao, N. Rega, G. Zheng, W. Liang, M. Hada, M. Ehara, K. Toyota, R. Fukuda, J. Hasegawa, M. Ishida, T. Nakajima, Y. Honda, O. Kitao, H. Nakai, T. Vreven, K. Throssell, J. A. Montgomery, Jr., J. E. Peralta, F. Ogliaro, M. Bearpark, J. J. Heyd, E. Brothers, K. N. Kudin, V. N. Staroverov, T. Keith, R. Kobayashi, J. Normand, K. Raghavachari, A. Rendell, J. C. Burant, S. S. Iyengar, J. Tomasi, M. Cossi, J. M. Millam, M. Klene, C. Adamo, R. Cammi, J. W. Ochterski, R. L. Martin, K. Morokuma, O. Farkas, J. B. Foresman, and D. J. Fox, Gaussian, Inc., Wallingford CT, 2016., (n.d.)..
[47] H.J.C. Berendsen, J.P.M. Postma, W.F. van Gunsteren, J. Hermans, Interaction models for water in relation to protein hydration, in: B. Pullman (Ed.), Intermolecular Forces, Springer Netherlands, Dordrecht, 1981, pp. 331–342, https://doi.org/10.1007/978-94-015-7658-1_21.
[48] Jmol: an open-source Java viewer for chemical structures in 3D. http://www.jmol.org/, (n.d.)..
[49] J. Liu, Q. Xu, J. Jiang, A molecular simulation protocol for swelling and organic solvent nanofiltration of polymer membranes, J. Membr. Sci. 573 (2019) 639–646, https://doi.org/10.1016/j.memsci.2018.12.035.
[50] E. Sireci, G. De Luca, J. Luque Di Salvo, A. Cipollina, G. Micale, Prediction of equilibrium water uptake and ions diffusivities in ion-exchange membranes combining molecular dynamics and analytical models, J. Membr. Sci. 668 (2023) 121283, https://doi.org/10.1016/j.memsci.2022.121283.
[51] M. Ding, A. Szymczyk, A. Ghoufi, Hydration of a polyamide reverse-osmosis membrane, J. Membr. Sci. 501 (2016) 248–253, https://doi.org/10.1016/j.memsci.2015.12.036.
[52] Q. Xu, J. Jiang, Computational characterization of ultrathin polymer membranes in liquids, Macromolecules 51 (2018) 7169–7177, https://doi.org/10.1021/acs.macromol.8b01387.
[53] D.A. Case, T.E. Cheatham, T. Darden, H. Gohlke, R. Luo, K.M. Merz, A. Onufriev, C. Simmerling, B. Wang, R.J. Woods, The Amber biomolecular simulation programs, J. Comput. Chem. 26 (2005) 1668–1688, https://doi.org/10.1002/jcc.20290.
[54] L. Shen, L. Li, J. Chen, H. Hong, H. Yu, Z. Hou, H. Lin, X. Lu, Effects of molecular weight distribution (Md) on the performances of the polyethersulfone (PES) ultrafiltration membranes, J. Membr. Sci. 490 (2015) 220–226, https://doi.org/10.1016/j.memsci.2015.04.068.
[55] L. Martínez, R. Andrade, E.G. Birgin, J.M. Martínez, PACKMOL: a package for building initial configurations for molecular dynamics simulations, J. Comput. Chem. 30 (2009) 2157–2164, https://doi.org/10.1002/jcc.21224.
[56] R.G. Gordon, Correlation functions for molecular motion, in: Adv. Magn. Opt. Reson., Elsevier, 1968, pp. 1–42, https://doi.org/10.1016/B978-1-4832-3116-7.50008-4.
[57] G. Rauhut, P. Pulay, Transferable scaling factors for density functional derived vibrational force fields, J. Phys. Chem. 99 (1995) 3093–3100, https://doi.org/10.1021/j100010a019.
[58] P. Pulay, G. Fogarasi, G. Pongor, J.E. Boggs, A. Vargha, Combination of theoretical ab initio and experimental information to obtain reliable harmonic force constants. Scaled quantum mechanical (QM) force fields for glyoxal, acrolein, butadiene, formaldehyde, and ethylene, J. Am. Chem. Soc. 105 (1983) 7037–7047, https://doi.org/10.1021/ja00362a005.
[59] S. Yang, M. Cho, IR spectra of N-methylacetamide in water predicted by combined quantum mechanical/molecular mechanical molecular dynamics simulations, J. Chem. Phys. 123 (2005) 134503, https://doi.org/10.1063/1.2038889.
[60] P. Wróbel, A. Eilmes, Effects of Me–solvent interactions on the structure and infrared spectra of MeTFSI (Me = Li, Na) solutions in carbonate solvents—a test of the GFN2-xTB approach in molecular dynamics simulations, Molecules 28 (2023) 6736, https://doi.org/10.3390/molecules28186736.
[61] P. Durlak, Z. Latajka, Car–Parrinello molecular dynamics and density functional theory simulations of infrared spectra for acetic acid monomers and cyclic dimers, Chem. Phys. Lett. 477 (2009) 249–254, https://doi.org/10.1016/j.cplett.2009.07.010.
[62] R. Singh, Hybrid Membrane Systems for Water Purification: Technology, Systems Design and Operation, Elsevier, Amsterdam Heidelberg, 2006, p. 1.
[63] C.A. Schneider, W.S. Rasband, K.W. Eliceiri, NIH Image to ImageJ: 25 years of image analysis, Nat. Methods 9 (2012) 671–675, https://doi.org/10.1038/nmeth.2089.
[64] M. Abunada, N. Dhakal, W.Z. Andyar, P. Ajok, H. Smit, N. Ghaffour, J.C. Schippers, M.D. Kennedy, Improving MFI-UF constant flux to more accurately predict particulate fouling in RO systems: quantifying the effect of membrane surface porosity, J. Membr. Sci. 660 (2022) 120854, https://doi.org/10.1016/j.memsci.2022.120854.
[65] S. Kadel, G. Pellerin, J. Thibodeau, V. Perreault, C. Lainé, L. Bazinet, How molecular weight cut-offs and physicochemical properties of polyether sulfone membranes affect peptide migration and selectivity during electrodialysis with filtration membranes, Membranes 9 (2019) 153, https://doi.org/10.3390/membranes9110153.
[66] C. Chen, H. Yang, X. Yang, Q. Ma, Tannic acid: a crosslinker leading to versatile functional polymeric networks: a review, RSC Adv. 12 (2022) 7689–7711, https://doi.org/10.1039/D1RA07657D.
[67] L.J. Karas, C. Wu, R. Das, J.I. Wu, Hydrogen bond design principles, WIREs Comput, Mol. Sci. 10 (2020) e1477, https://doi.org/10.1002/wcms.1477.
[68] T. Steiner, The hydrogen bond in the solid state, Angew. Chem. Int. Ed. 41 (2002) 48–76, https://doi.org/10.1002/1521-3773(20020104)41:1<48::AID-ANIE48>3.0.CO;2.
[69] T.F. Headen, C.A. Howard, N.T. Skipper, M.A. Wilkinson, D.T. Bowron, A.K. Soper, Structure of π−π interactions in aromatic liquids, J. Am. Chem. Soc. 132 (2010) 5735–5742, https://doi.org/10.1021/ja909084e.
[70] Y. Ma, A.L. Zydney, R. Wang, J.W. Chew, Molecular dynamics study on membrane fouling by oppositely charged proteins, AIChE J. 67 (2021), https://doi.org/10.1002/aic.17335.Appendice.